Applied Thermal Engineering 88 (2015) 118–126

Contents lists available at ScienceDirect

Applied Thermal Engineering

journal homepage: www.elsevier.com/locate/apthermeng

Research paper

Influence of heater thermal capacity on bubble dynamics and heat transfer in nucleate pool boiling

Liang Zhang [a, c], Zhen-Dong Li [a], Kai Li [a], Hui-Xiong Li [b], Jian-Fu Zhao [a, *]

[a] Key Laboratory of Microgravity (National Microgravity Laboratory)/CAS, Institute of Mechanics, Chinese Academy of Sciences (CAS), Beijing 100190, China
[b] State Key Laboratory of Multiphase Flow in Power Engineering, Xi'an Jiaotong University, Xi'an 710049, China
[c] State Nuclear Power Software Development Center (SNPSDC), Beijing 102209, China

HIGHLIGHTS

- Complete simulations of single bubble pool boiling including transient thermal response of solid wall are performed.
- The Ghost Fluid Method (GFM) is used for sharp interface representation.
- Influences of heater thermal capability on bubble thermal dynamics and heat transfer are carried out.

ARTICLE INFO

Article history:
Received 19 June 2014
Received in revised form
23 October 2014
Accepted 15 November 2014
Available online 12 December 2014

Keywords:
Single bubble pool boiling
Transient thermal response of solid wall
Bubble dynamics
Heat transfer

ABSTRACT

Using the Ghost Fluid Method for sharp interface representation, the complete single bubble pool boiling process including the transient thermal response of the solid wall is simulated numerically. Two level set functions are used for capturing the liquid–vapor–solid interfaces. Bubble dynamics and local heat transfer influenced by thickness and material parameters of the solid wall are analyzed at constant temperature on its bottom. For the same material and the same bottom temperature, growth time and departure diameter of bubble change slightly with the thickness. A clear local low-temperature region is produced inside the wall under the bubble base, which expands and recedes periodically with the movement of the three phase contact line. The movement of the local low-temperature region lags gradually comparing to that of the contact line with increasing thermal diffusivity of solid walls. Waiting time increases with decreasing thermal diffusivity of solid walls, resulting in thickened thermal boundary layer at nucleation, and then short bubble growth time and large departure diameter.

1. Introduction

It is believed that the quasi–periodic cycle of bubble growth, departure, and waiting processes plays a fundamental role in nucleate pool boiling. When the superheat of nucleate site reaches a certain critical value, an initial bubble will form. The bubble then grows by absorbing heat from the solid wall underneath it and the surrounding superheated liquid. Furthermore, it is well known that a very thin liquid microlayer forms under the growing bubbles. Moore & Mesler [1] and Cooper & Lloyd [2] indicated firstly the existence of the microlayer beneath the bubble through the measurement of local temperature on the heating surface, and noted evaporation of the microlayer has an important role. Because of the heat removed from the microlayer nearby the three phase contact line, the temperature in the vicinity of the nucleate site will drop greatly. When the bubble grows big enough, forces acted upon it, mainly the buoyancy in a gravitational field, will make it departure from the heating surface. Then the nucleate site will go through a recovering or waiting process until its superheat reaches the critical value and a new subsequent bubble forms again. Thus, evaporation of the microlayer, heat conduction inside the solid wall of the heater, local fluid flow and heat transfer around the growing bubble will have significant effects on bubble thermal dynamics and heat transfer of nucleate pool boiling.

With the progress of advanced measurement technique in recent years, some experimental data on the microlayer with high temporal and/or spatial resolutions become available. Jung & Kim [3] measured simultaneously the microlayer shape by the total internal reflection (TIR) technique, and the temperature distribution on the heating surface by a high-speed, high-resolution

* Corresponding author. Tel.: +86 10 82544129.
E-mail address: jfzhao@imech.ac.cn (J.-F. Zhao).

http://dx.doi.org/10.1016/j.applthermaleng.2014.11.080
1359-4311/

Nomenclature

A	area
C_p	specific heat
D	diameter
g	gravity vector
H	heaviside function
h	grid size
h_{ev}	interfacial thermal resistance
h_{fg}	latent heat
k	thermal conductivity
L	characteristic or Laplace length
$\dot{m}$	mass flux
$\mathbf{n}$	normal vector
p	pressure
q	heat flux
R_1	end position of microlayer
R_0	three phase contact point
T	temperature
t	time
$\mathbf{t}$	tangential vector
U	characteristic velocity
$\mathbf{u}$	velocity vector
V	volume
ΔT	superheat

Greece symbols

α	thermal diffusion
β_T	interfacial thermal expansion
γ	contact angle
δ	thickness of microlayer
δ_T	thermal boundary layer thickness
θ	characteristic temperature
κ	curvature
μ	dynamic viscosity
ν	kinematic viscosity
ρ	density
σ	surface tension
τ	dimensionless time
φ	level set function for vapor–liquid interface
ψ	level set function for liquid–solid interface
Ω	phase domain
Γ	interface between phases

Subscripts

d	departure
f	fluid
h	heater
int	interface
l	liquid
mic	micro-region
n	nucleation
o	beginning of bubble cycle
s	solid wall
sat	saturation
v	vapor
w	wall or waiting time
ave	spatio-temporal averaged

infrared (IR) thermometry. They reported a wedge-shaped microlayer, and nearly the same values of advancing and receding contact angle. Utaka et al. [4] used a laser extinction method to measure the microlayer structure in nucleate boiling. They also found that the microlayer is shaped like a wedge. For a fixed position, the microlayer thickness decreased over time due to evaporation, and the thickness of the initially formed microlayer increased linearly with increasing distance between the incipient bubble site and the measurement position. The relationship is independent of the heat flux, but varies with the working fluid.

To reveal the mechanism underlying the pseudo-periodic bubble cycle, several models have been proposed to model the local fluid flow and heat transfer of single bubble pool boiling in the literature. Among them, the model proposed by Stephan & Hammer [5] is the most often used one. In this model, a fourth order differential equation is derived for the microlayer by using the lubrication theory accompanying the Young–Laplace equation, as well as the kinetic theory of gases with the Clausius–Clapeyron equation to model the evaporation rate from the vapor–liquid interface. The equation can be solved to obtain the liquid film thickness, the local heat flux, and so on. They showed that the interface of the microlayer has a nearly constant slope except the vicinity of the adhesion region where the slope decreases to zero rapidly. Following the model of Stephan & Hammer [5], single bubble boiling phenomenon with major focus upon bubble behaviors and heat transfer was numerically simulated by many researchers [6–17]. For simplicity in the most of studies, however, the influence of transient heat conduction inside the solid wall is often ignored, in which a constant temperature is adopted for the boundary condition instead of the actual solid wall of the heater.

On the contrary, many experimental studies showed that the temperature on the heating surface can vary both temporally and spatially during the boiling process. An experimental investigation of saturated water pool boiling at atmospheric pressure on thin, horizontal, cylindrical walls by Magrini & Nannel [18] showed that a higher heat transfer coefficient was obtained with the increasing of thermal diffusivity of the solid wall and/or decreasing of its thickness. Kenning & Yan [19] studied the nucleate pool boiling of water on a thin plate with 0.13 mm thickness by using the thermochromic technology. They reported that the amplitude of the consequent wall temperature variations depends on the thickness and thermal properties of the heated solid wall. Fischer et al. [20] conducted boiling experiments under low gravity condition which allowed temperature measurements by high-speed infrared thermography. During the bubble growth process, the local cold area was changed with the moving of the microlayer, and a distinct local temperature drop about 4 K can be observed. Similar results were also reported by Yabuki & Nakabeppu [21] by using MEMS sensors with high temporal and/or spatial resolution in temperature measurement. Thus, numerical models for the processes of bubble nucleation and growth with a uniform wall superheat cannot be realistic.

Mei et al. [7] carried out a numerical analysis of the bubble growth in saturated pool boiling. They analyzed that the time scale required for the solid wall to adjust its temperature into a uniform distribution for most boiling systems is much longer than the bubble departure time. Therefore, the actual bubble growth rate should be smaller than that predicted by assuming a constant wall temperature. Mann et al. [8] simulated the influence of heat conduction in the wall, of which the wall thermal conductivity was set to the values of copper, stainless steel and a ceramic material. Only moderate influence was observed, caused by the following effects partly compensating: the local heat flux decreases on the solid wall with lower thermal conductivities, while, on the other hand, lower

thermal conductivities lead to thinner liquid films in the micro region which enhances heat conduction in the film and causes higher heat fluxes. To evaluate the influence of transient heat conduction, heat storage, and convection in liquid and wall on overall heat transfer, Fuchs et al. [11] calculated heat flow through different interfaces, e.g. wall-liquid and/or liquid–vapor, of the single bubble subsystem. It was found that the variation of heat stored in the wall is significant, although the thermal inertia of the wall is rather small. Kunkelmann & Stephan [13] simulated the nucleate boiling of refrigerant HFE-7100 on a steel foil with a thickness of 50 μm. They observed that the heater is cooled down locally and a peak of heat flux is evident near the contact line. Aktinol & Dhir [15], however, found that the results without the effect of transient thermal response of wall only slightly over-predicted the rate of heat removal. Nam et al. [17] further studied the effect of varying contact angle on the thermal response of the solid during nucleate pool boiling. It was shown that the heat transfer coefficient increases very weakly with increasing contact angle, while thicker surface shows slightly larger effect of contact angle on heat transfer coefficient. In our previous work (Zhang et al. [16]), single bubble pool boiling including transient thermal response of solid wall was simulated numerically by using the ghost fluid method and the level set method for the sharp interface representation. Two different nucleate criteria, namely constant waiting time and constant nucleate superheat, were used for determining the appearance time for the subsequent bubble. The results verified their consistency in nature.

Decoupling the fluid by using the normalization of measurement results of microlayer characteristics, Utaka et al. [22] calculated the 2-D heat transfer characteristics in a heating plate during the process of microlayer evaporation. It was confirmed that the temperature of the heating surface decreased with microlayer evaporation and reach a minimum at a certain time, and then recovered after bubble departure. They concluded that the enthalpy stored in the heating plate within the distance less than the penetration depth was consumed by microlayer evaporation through unsteady thermal conduction, while the heat flux from the bottom of the heating plate had a little effect on the microlayer evaporation rate but mainly determined the length of a bubble cycle as a time-averaged heat supply.

In the present study, a further numerical study of our previous work (Zhang et al. [16]) on the influence of heater thermal capability on bubble thermal dynamics and heat transfer in single bubble pool boiling will be carried out, using the Ghost Fluid Method (GFM) for the sharp interface representation and two level set functions for capturing the liquid–vapor–solid interfaces. Considering the transient thermal response of the solid wall, major aims of the present study are focused upon the effects of the wall thickness, thermal properties, and the size of nucleate site, on the bubble growth process, local heat transfer both in the fluid and in solid wall, and so on.

2. Numerical model

Following Stephan & Hammer [5], the computational domain for single bubble pool boiling process is divided into micro and macro regions (Fig. 1). The following assumptions are made during the present study: 1) the fluid in each phase is Newtonian, viscous and incompressible; 2) the material properties are constant and not influenced by the temperature and pressure; 3) the flow in fluid phases is axisymmetric and laminar, while the heat conduction inside the solid wall is also axisymmetric; 4) the apparent contact angle is constant; 5) a constant temperature is maintained on the bottom of the solid wall.

The continuity, momentum, energy conservation equations for the macro region are written as

$$\mathbf{u} = 0, \quad \Omega_s \tag{1}$$

$$\nabla\cdot\mathbf{u} = 0, \quad \Omega = \{\Omega_v \cup \Omega_l\} \tag{2}$$

$$\rho\left(\frac{\partial\mathbf{u}}{\partial t} + \mathbf{u}\cdot\nabla\mathbf{u}\right) = -\nabla p + \nabla\cdot\mu(\nabla\mathbf{u} + \nabla\mathbf{u}^T) + \rho[1-\beta_T(T-T_{\text{sat}})]\mathrm{g}, \quad \Omega = \{\Omega_v \cup \Omega_l\} \tag{3}$$

$$\begin{cases} \dfrac{\partial T}{\partial t} + \mathbf{u}\cdot\nabla T = \dfrac{1}{\rho C_p}\nabla\cdot k(\nabla T), & \Omega = \{\Omega_l \cup \Omega_s\} \\ T = T_{\text{sat}}(p_v), & \Omega_v \end{cases} \tag{4}$$

The conservation equations are solved accompanied with the jump conditions [16,23] at the interface

$$[\mathbf{u}]_\Gamma = \begin{cases} -[1/\rho]_\Gamma \dot{m}\mathrm{n}, & \Gamma_{lv} \\ 0, & \Gamma_{fs} \end{cases} \tag{5}$$

$$[\mu(\nabla u\cdot\mathrm{n}, \nabla v\cdot\mathrm{n})\cdot\mathrm{t} + \mu(\nabla u\cdot\mathrm{t}, \nabla v\cdot\mathrm{t})\cdot\mathrm{n}]_\Gamma = 0, \quad \Gamma_{lv} \tag{6}$$

$$[p]_\Gamma = 2[\mu(\nabla u\cdot\mathrm{n}, \nabla v\cdot\mathrm{n})\cdot\mathrm{n}]_\Gamma - \sigma\kappa - [1/\rho]_\Gamma \dot{m}^2, \quad \Gamma_{lv} \tag{7}$$

$$[T]_\Gamma = 0, \quad \Gamma_{lv} \tag{8}$$

$$[k\nabla T\cdot\mathrm{n}]_\Gamma = \begin{cases} \dot{m}h_{fg}, & \Gamma_{lv} \\ 0, & \Gamma_{fs} \end{cases} \tag{9}$$

where the jump across the interface is defined as $[\Lambda]_\Gamma = \Lambda_l - \Lambda_v$ for Γ_{lv} and $[\Lambda]_\Gamma = \Lambda_f - \Lambda_s$ for Γ_{fs}, and the mass flux $\dot{m}$ is defined as $\dot{m} = \rho(\mathbf{u}_{\text{int}} - \mathbf{u})\cdot\mathrm{n}$.

In the present paper, the assumption of constant interface slope for the axisymmetric micro region [3,9] is adopted, namely

$$\frac{\mathrm{d}\delta}{\mathrm{d}r} = \tan\gamma \tag{10}$$

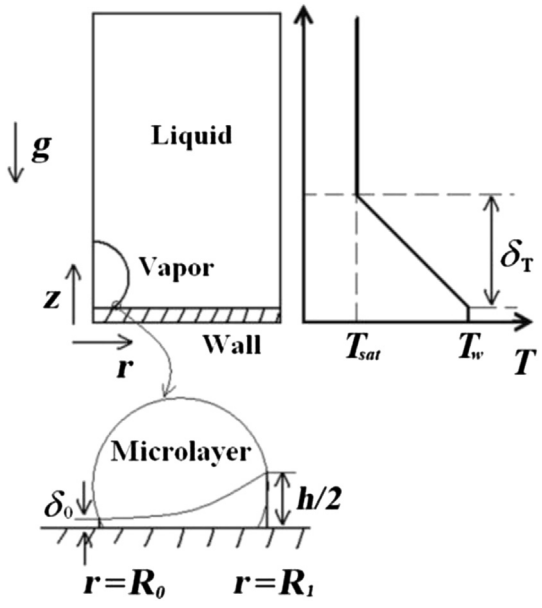

Fig. 1. Computational domain used in the numerical simulation.

where γ denotes the apparent contact angle. Thus, based on the combination of the mass, momentum, and energy equations for the micro region, formulations for the area averaged heat flux q_{mic} and mass flux $\dot{m}_{\text{mic}}$ of the micro region is obtained, respectively [14]

$$q_{\text{mic}} = \frac{2\pi k_l (T_w - T_{\text{sat}})}{\Delta A_{\text{mic}}} \left[\left(R_1 - \frac{h}{2\tan\gamma} \right) \frac{1}{\tan\gamma} \ln\left(\frac{h}{2} \frac{h_{ev}}{k_l} + 1 \right) + \frac{h}{2\tan^2\gamma} - \frac{k_l}{h_{ev}} \frac{1}{\tan^2\gamma} \ln\left(\frac{h}{2} \frac{h_{ev}}{k_l} + 1 \right) \right] \tag{11}$$

$$\dot{m}_{\text{mic}} = \frac{q_{\text{mic}}}{h_{fg}} \tag{12}$$

Two level set functions are used for capturing the liquid–vapor–solid interfaces. Firstly, the liquid–vapor interface is advanced by solving the following equation

$$\frac{\partial \varphi}{\partial t} = -\mathbf{u}_{\text{int}} \cdot \nabla \varphi \tag{13}$$

where $\mathbf{u}_{int}$ is the interface velocity, which is defined as

$$\mathbf{u}_{\text{int}} = \frac{\dot{m}\mathbf{n}}{\rho} + \mathbf{u} \tag{14}$$

Reinitialization is needed to maintain a signed distance function from the interface

$$\varphi_\tau + S(\varphi_0)(1 - |\varphi|) = 0 \tag{15}$$

where the smoothed out sign function $S(\varphi_0) = \varphi_0 / \sqrt{\varphi_0^2 + \Delta x^2}$, and φ_0 is the solution of Eq. (13).

Another level set function ψ is also used to treat the immersed solid surface which is defined as a signed distance from the fixed fluid–solid interface. The level set function ψ is not necessary to be advanced.

The material properties of different phases are described as

$$\rho = \rho_s + [\rho_v + (\rho_l - \rho_v) H(\varphi) - \rho_s] H(\psi) \tag{16}$$

$$\mu = \mu_s + [\mu_v + (\mu_l - \mu_v) H(\varphi) - \mu_s] H(\psi) \tag{17}$$

$$k^{-1} = k_s^{-1} + \left[k_l^{-1} H(\varphi) - k_s^{-1} \right] H(\psi) \tag{18}$$

where H is the discontinuous Heaviside function, which is described as

$$H = \begin{cases} 1 & \text{if } \varphi \text{ or } \psi > 0 \\ 0 & \text{if } \varphi \text{ or } \psi \le 0 \end{cases} \tag{19}$$

The computational domain of the fluid was chosen to be (1L, 2L), in order for that the process of bubble growth is not affected by the computational boundary. The boundary conditions used in the present simulation are as follows.

At the axis of symmetry,

$$u = \frac{\partial v}{\partial r} = \frac{\partial T}{\partial r} = \frac{\partial \varphi}{\partial r} = 0 \tag{20}$$

At the right of domain,

$$u = \frac{\partial v}{\partial r} = \frac{\partial T}{\partial r} = \frac{\partial \varphi}{\partial r} = 0 \tag{21}$$

At the bottom of the wall,

$$u = v = 0, \quad T = T_w \tag{22}$$

At the top boundary,

$$\frac{\partial u}{\partial z} = \frac{\partial v}{\partial z} = \frac{\partial \varphi}{\partial z} = 0, \quad T = T_{\text{sat}} \tag{23}$$

Another two conditions in the vicinity of three-phase contact line inside the wall also need to be considered

$$\left(k \frac{\partial T}{\partial z} \right)_{\text{mic}} = -q_{\text{mic}}, \quad \frac{\partial \varphi}{\partial z} = -\cos\gamma \tag{24}$$

The primary variables is non-dimensioned by the following characteristic scales

$$L = \sqrt{\frac{\sigma}{g(\rho_l - \rho_v)}}, \quad U = \sqrt{gL} \quad t_0 = \frac{L}{U} \tag{25}$$

and the dimensionless temperature is defined as $\theta = T - T_{\text{sat}} / T_w - T_{\text{sat}}$.

Initial still flow field is used as the initial velocity condition, namely

$$u = v = 0 \text{ at } t = 0 \tag{26}$$

While the initial thermal distribution is given as shown in Fig. 1, where the initial thermal boundary-layer thickness is determined by the correlation [24]

$$\delta_T = 7.14 \left(\frac{\nu_l \alpha_l}{g \beta_T \Delta T} \right)^{1/3} \tag{27}$$

A small truncated spherical bubble with the initial radius of $0.05L$ is set on the top surface of the solid wall at the beginning of a bubble cycle. Constant nucleating superheat corresponding to the given cavity diameter, D_c, of the nucleate site [25]

$$\Delta T_n = T_w - T_{\text{sat}} = \frac{4 f_1 \sigma T_{\text{sat}}}{D_c h_{fg} \rho_v} \Big/ \left(1 - \frac{f_2 D_c}{2 f_1 \delta_T} \right) \tag{28}$$

is chosen as the criterion for determining the beginning of the subsequent bubble cycle, where f_1 and f_2 are functions of the contact angle.

A standard MAC grid is used for the spatial discretization where the velocities are defined at the grid surfaces and other variables are defined at the grid nodes. The projection method is used to numerically solve the Navier–Stokes equations. The 2nd order ENO scheme is used for discretization of the convection term in the momentum and energy equations, and the central difference is used for the diffusion terms. For more details about the level set method, including the related solving procedure and algorithm, one can see Zhao et al. [26,27] and Zhang et al. [28]. Multi cycle of bubble growth computations are adopted for all cases below till a steady state is reached.

Some validation works of present numerical method can be found in Zhao et al. [14], Zhang et al. [16], and Zhang [29]. The numerical results of the present numerical method have been compared both with the experimental results of Siegel & Keshock [30] and with the numerical results of Son [9] and Son et al. [10]. Good agreements were evident.

3. Results and discussion

Three kinds of materials, namely fused silica (SiO_2), nickel (Ni), and stainless steel (SS), which are commonly applied in engineering, are studied in the present work, and their materiel parameters

are listed in Table 1. Furthermore, fused silica will be used as the substrate of an integrated heater in our on-going space experiment mission, SOBER-SJ10, which will be flown of our group, to study local convection and heat transfer around an isolated growing vapor bubble during nucleate pool boiling on a flat plate heater (Hu et al. [31]). Nickel was used by Siegel & Keshock [30] in their experiments, and, as mentioned above, their experimental results were used to validate the present numerical method.

The working fluid used in the present study is saturated water at 0.1 MPa. A nominal superheat $\Delta T_w = 6.17$ K on the heater's bottom is used in all cases. As shown in Eq. (10), contact angle plays an important role on the bubble growth process and microlayer under the growing bubbles. Zhao et al. [14], as well as Nam et al. [17], studied numerically this effect in detail. The present study, however, focuses on the influence of heater thermal capacity, so only a constant apparent contact angle, *i.e.* 38°, on the top surface of the solid wall is used in the numerical simulation.

Table 2 summarizes the results of single bubble pool boiling in different cases. In the present simulations, a constant temperature boundary condition is adopted on the bottom of solid walls. Thus, both the time-space averaged heat flux q_{ave} and superheat $\Delta T_{w,ave}$ over the surface of wall during a whole bubble cycle are not controllable variables but dependent ones, which are also listed in Table 2.

It can be seen from Table 2 that, for the cases of the same material of the solid wall (SiO_2), bubble growth time t_g decreases slightly, while the departure diameter D_d increases with the increase of wall thickness. However, the waiting time t_w is prolonged intensively with the increase of wall thickness. Besides, both the time-space averaged superheat and heat flux decreases with the increase of wall thickness, which can be deduced straightforwardly from the different resistance of heat conduction across the solid wall with different thickness.

The dependency of bubble behaviors and heat transfer characteristics on the wall thickness can be explained in detail by the flow and temperature fields shown in Fig. 2 (depicted by the same length scale), in which results of three cases of bubble growth on SiO_2 wall with thickness of 0.5, 1.0, and 1.5 mm are presented in three columns, respectively. A clear local low-temperature region, or a thermal "hollow", is produced inside the solid wall underneath the bubble base, which has a periodical expanding and receding feature because of the movement of contact line, and relevant evaporation of microlayer and transient heat conduction inside the solid wall. Besides, comparing with the movement of the contact line on the fluid–solid interface, lag effect of the movement of the local low-temperature region inside the solid wall can be seen as another obvious characteristic, particularly in the receding stage. It is caused by the unsteady heat conduction inside the solid wall, which is caused by the quasi-alternating temperature condition on the fluid–solid interface. The corresponding governing equation is a parabolic partial differential equation with independent variables of time and position. Thus, inside the solid wall, the temperature variety exhibits a time lag comparing with that occurred on the fluid–solid interface, and its amplitude attenuates with the increase of the distance away from the interface, resulting in a penetration depth over which the temperature variety becomes small enough to be neglected. It is clearly shown in Fig. 2 that, inside the solid wall, the temperature field far away from the area covered by the growing bubble may keep in the steady state. In addition, the vector field of temperature gradient at departure of bubble is also presented in Fig. 2. It is evident that the relatively stronger heat consumption only occurs in the vicinity of the solid–liquid–vapor contact region. It is obvious that the recovery of the temperature on the nucleate site and the thermal boundary layer near the heating surface is influenced by heat conduction inside the solid wall, and then the transient heat transfer and the periodical thermal storage and release inside the solid wall can affect evidently bubble thermal dynamics and heat transfer.

Table 1
Material properties of solid walls.

Material	Fused silica (SiO_2)	Stainless steel (SS)	Nickel (Ni)
Density ρ (kg/m^3)	2220	7900	8870
Specific heat C_p (J/kg K)	865	505.5	478.5
Thermal conductivity k (W/m K)	1.4775	16.175	82.75
Thermal diffusivity α ($\times 10^{-6}$ m^2/s)	0.77	4.05	19.49

Table 2
Simulation results of single bubble pool boiling in different cases.

Material	ΔT_n (K)	D_c (m)	h_w (mm)	t_g (ms)	t_w (ms)	D_d (mm)	$\Delta T_{w,ave}$ (K)	q_{ave} (W/cm^2)
SiO_2	4.1	1×10^{-5}	0.5	32.3	103.0	2.55	4.31	0.522
SiO_2	4.1	1×10^{-5}	1.0	32.1	405.0	2.59	4.05	0.396
SiO_2	4.1	1×10^{-5}	1.5	31.5	3789	2.61	4.00	0.390
SS	4.1	1×10^{-5}	1.0	33.8	8.147	2.40	5.22	1.192
Ni	5.1	8×10^{-6}	1.0	32.8	0.732	2.41	5.68	1.660

Fig. 3 shows the evolutions of bubble shape and its movement, the temperature and flow fields around the bubble during some typical multi cycles after the pseudo-steady state of quasi-periodical bubble cycle is reached. Compared with our early work (Zhang et al. [16]), the time for recovering the temperature at the nucleate site is decreased due to the decreased nucleate superheat for a bigger cavity size in this case, which results in increased bubble re-birth frequency and then vertical merger of consecutive bubbles. A larger bubble is pinched off by surface tension force quickly. Simultaneously, some little liquid drops may be carried into the bubble by large interfacial deformation at the bottom of merged bubble. Son et al. [10] also reported some numerical and experimental results of vertical merger on a single nucleation site. Despite of different operating conditions, similar topological evolutions are evident between the present results and those reported by Son et al. [10].

Comparison among the results with different materials is also presented in Table 2. It should be noted firstly that the nucleate superheat ΔT_n is calculated to be 4.1 K for the cavity size of nucleate site $D_c = 1 \times 10^{-5}$ m based on Eq. (28). No waiting period, however, exists in the case of Ni due to its high thermal diffusivity. Thus, a new value of nucleate superheat $\Delta T_n = 5.1$ K, corresponding to $D_c = 8 \times 10^{-6}$ m, is adopted in the case Ni. It can be observed that both the time-space averaged superheat and heat flux on the heating surface increases with the thermal diffusivity of solid wall, while the waiting time decreases dramatically. Except the case of Ni, bubble growing time increases with the thermal diffusivity of solid wall, while the departure diameter decreases. Due to modified nucleate superheat in the case of Ni as mentioned above, no regular tendency of bubble growth exhibits comparing with the other two cases.

A comparison of bubble growth on heaters with different materials during a typical bubble cycle is shown in Fig. 4. The evolutions of bubble interface in discrete time points are shown in the first row. To reveal the development of the thermal boundary layers on different solid walls, temperature fields are also shown only at the end of the bubble cycles or the beginning of the subsequent one for clarity. To simplify the description of bubble growth pattern, the same time scale is used in the horizontal coordinates. It can be seen that the thermal boundary layer is thickened much better with the increase of waiting time.

In the second row of Fig. 4, the changes of temperature at the nucleate site on different solid walls are presented. Twice

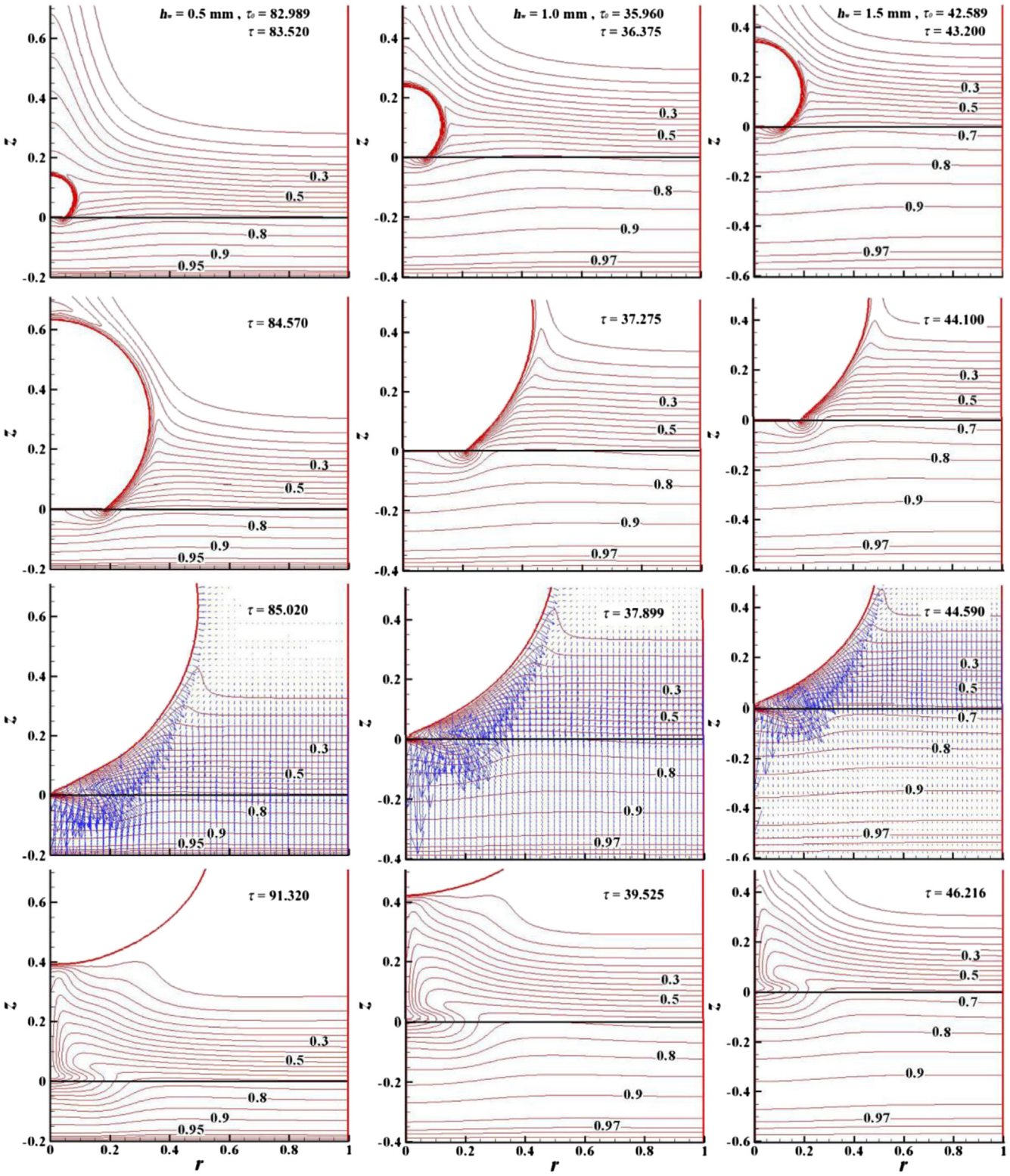

Fig. 2. Evolution of bubble growth and dimensionless temperature field on SiO_2 with different thickness. The wall thickness, as well as the beginning of the shown bubble cycles, of each column is marked in the corresponding subplots in the upper row, while the corresponding time is also marked in each subplot.

temperature drops occur in all curves. The first drop is smaller and lasts for a very short period, which is not coincident with experimental observation. The reason rests on the simplified assumption in the present model that a small truncated spherical bubble is used for the initial bubble instead of the actual nucleation process. Then violent heat absorbing from the surroundings in the inertia-controlled stage of the initial bubble growth cannot be simulated. Small amount of heat is absorbed to maintain the growth of the initial small bubble, and thus only a smaller temperature drop at the nucleate site is obtained here. Along with the bubble growth,

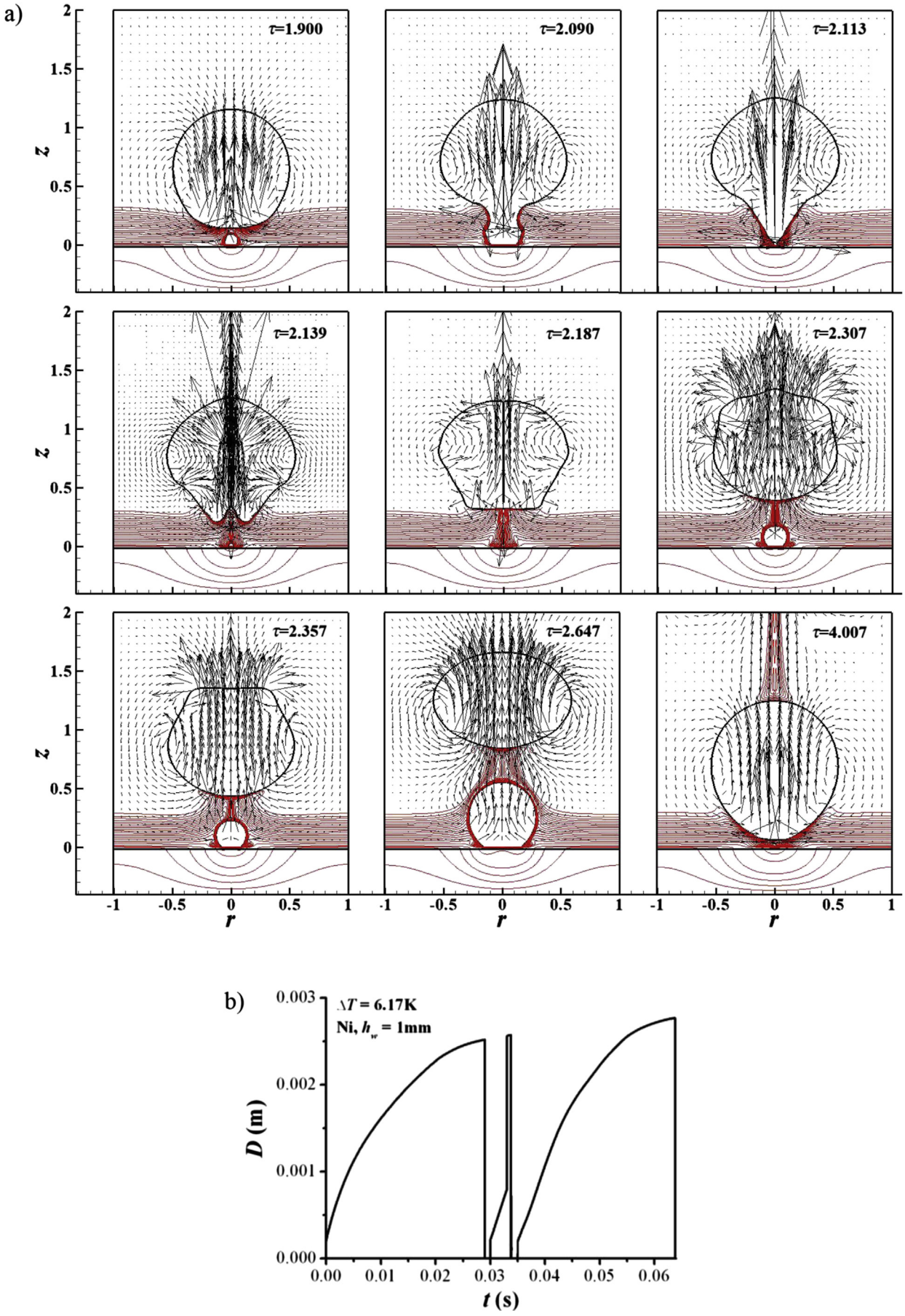

Fig. 3. a) Bubble growth with bigger cavity size (Ni, $h_w = 1$ mm, $D_c = 1 \times 10^{-5}$ m). b) The isotherm interval is 0.05 in solid wall, while 0.01 in fluid.

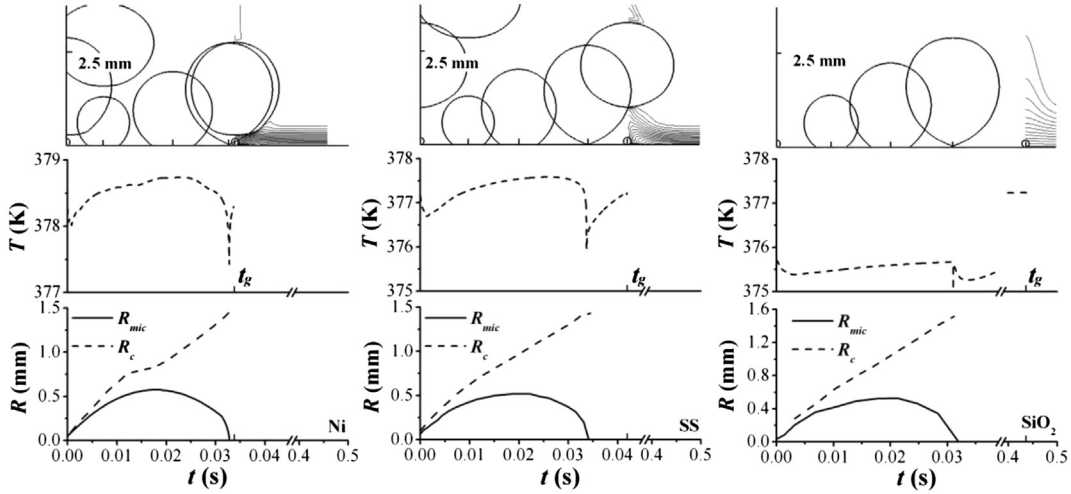

Fig. 4. Bubble growth on the heater with different material ($h_w = 1$ mm). The upper row: bubble growth process during a typical bubble cycle; the middle row: the changes of temperature at the nucleate site; and the lower row: the changes of bubble base radius (R_{mic}) and height of bubble mass center (R_c). The wall material of each column is marked in the corresponding subplots in the lower row.

the bubble base extends and a local dry-spot emerges after the microlayer passes by. The nucleate site is heated again, resulting in the temperature increase. The heating stage will be ended when the contact line recedes and the liquid re-floods on the local dry-spot, and thus, a secondary temperature drop occurs. After bubble departure, the temperature rises again until the nucleate criterion reaches again. In the case of SiO_2, however, a small drop exhibits shortly after the bubble departure, which reflects the lag effect of the movement of the local low-temperature region, which is mentioned above. The smaller thermal diffusivity of solid wall is, the larger lag effect can be observed.

The changes of the bubble base radius and the height of bubble mass center are given in the last row of Fig. 4. The uplifted velocity of the bubble mass center is kept approximately to be constant at first, and then it experiences a transition before the maximum radius of bubble base is reached for all kinds of heaters. The transition is more obvious in the case of Ni. This may be caused by the different thermal diffusivity of solid walls, and corresponding differences on the development of the thermal boundary layer and the transient thermal response of solid walls. Although the bubble growth times in the three cases are similar, a stronger thermal diffusion inside solid wall may be corresponding to a shorter waiting time under the same nucleate criterion (see also Table 2), and then a thinner thermal boundary layer. Thus, if the thermal boundary layer in liquid is not recovered enough due to quick recovery of temperature inside solid wall with larger thermal diffusivity, the energy stored in the thermal boundary layer may not be enough to maintain a steady growth of bubble, and then the transition occurs when the bubble grows out of the superheated liquid layer. Furthermore, a slower growth rate will be obtained.

More detail of the temperature distribution and the vector field of temperature gradient at the bubble departure on different solid walls are given in Fig. 5. Two important aspects of the thermal boundary layer on the heating surface can be observed. It plays an important role in supplying heat for the growth of bubble, as well as in removing heat directly into liquid from the heating surface. Far away from the nucleate site, the temperature gradient along the heating surface decreases with decreasing thermal diffusivity, which means that the heat removed directly into liquid from the heating surface is reduced, and then the evaporation will be in the ascendant in removing heat from the solid wall. It is also clearly shown that due to the transient heat respond of heater and the backflow of cold liquid around the bubble base, the movement of the local low-temperature region lags gradually comparing to that of the contact line with increasing thermal diffusivity of solid walls.

4. Conclusions

Using the Ghost Fluid Method for sharp interface representation, the complete single bubble pool boiling processes including the transient thermal response of the solid wall are numerically simulated. In the simulation, both the time-space averaged heat

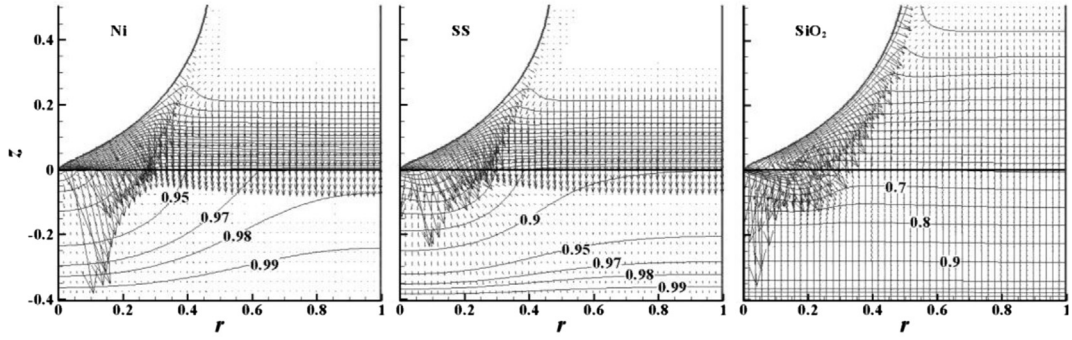

Fig. 5. Temperature distribution and vector of temperature gradient at bubble departure ($h_w = 1$ mm).

flux and superheat on the surface of solid wall are not controllable but dependent variables. It is obvious that bubble growth time decreases with the wall thickness, while the departure diameter increases. However, waiting time is prolonged much intensively.

A clear local low-temperature region is produced inside solid wall under the bubble base. It has a periodical expanding and receding feature because of the movement of contact line, and relevant evaporation of microlayer and transient heat conduction inside the solid wall. The movement of the local low-temperature region lags gradually comparing to that of the contact line with increasing thermal diffusivity of solid walls.

Waiting time increases with decreasing thermal diffusivity of solid walls, which results in a thickened thermal boundary layer at nucleation. And then, bubble growth time is shortened and departure diameter is increased. The vertical velocity of bubble growth is kept approximately to be constant at first, and then it experiences a transition before the maximum radius of bubble base is reached for all kinds of heaters. The transition is more obvious in the case of Ni, which may also be caused by the different thermal diffusivity of solid walls, and corresponding differences on the development of the thermal boundary layer and the transient thermal response of solid walls.

Two important aspects of the thermal boundary layer on the heating surface can be observed. It supplies heat for the growth of bubble, and removes heat directly into liquid from the heating surface. The latter will be weakened with decreasing thermal diffusivity, and then the evaporation will be in the ascendant in removing heat from the solid wall for low thermal diffusivity case.

Acknowledgement

The present study is supported financially by the National Natural Science Foundation of China under the grants of 11372327 and 10972225, and the Strategic Priority Research Program on Space Science, the Chinese Academy of Sciences under the grants of XDA04020404 and XDA04020202-04. The authors also appreciate Prof. Li Yuan (Academy of Mathematics and Systems Science, CAS), and Prof. Zai-Sha Mao (Institute of Process Engineering, CAS) for fruitful discussions.

References

[1] F.D. Moore, R.B. Mesler, The measurement of rapid surface temperature fluctuations during nucleate boiling of water, AIChE J. 7 (1961) 620–624.
[2] M.G. Cooper, A.J.P. Lloyd, The microlayer in nucleate pool boiling, Int. J. Heat Mass Transfer 12 (1969) 915–933.
[3] S. Jung, H. Kim, Synchronized measurement of liquid–vapor phase and temperature distributions on a boiling surface during single bubble nucleate boiling. 8th International Conference on Multiphase Flow (ICMF 2013), Jeju, Korea, May 26–31, 2013.
[4] Y. Utaka, Y. Kashiwabara, M. Ozaki, Microlayer structure in nucleate boiling of water and ethanol at atmospheric pressure, Int. J. Heat Mass Transfer 57 (2013) 222–230.
[5] P. Stephan, J. Hammer, A new model for nucleate boiling heat transfer, Heat Mass Transfer 30 (1994) 119–125.
[6] J.H. Lay, V.K. Dhir, Shape of a vapor stem during nucleate boiling of saturated liquids, J. Heat Transfer 117 (1995) 394–401.
[7] R. Mei, W. Chen, J.F. Klausner, Vapor bubble growth in heterogeneous boiling-I, Formulation. Int. J. Heat Mass Transfer 38 (5) (1995) 909–919.
[8] M. Mann, K. Stephan, P. Stephan, Influence of heat conduction in the wall on nucleate boiling heat transfer, Int. J. Heat Mass Transfer 43 (2000) 2193–2203.
[9] G. Son, Numerical study on a sliding bubble during pool nucleate boiling, KSME Int. J. 15 (7) (2001) 931–940.
[10] G. Son, N. Ramanujapu, V.K. Dhir, Numerical simulation of bubble merger process on a single nucleation site during pool nucleate boiling, J. Heat Transfer 124 (2002) 51–62.
[11] T. Fuchs, J. Kern, P. Stephan, A transient nucleate boiling model including microscale effects and wall heat transfer, J. Heat Transfer 128 (2006) 1257–1265.
[12] D. Li, V.K. Dhir, Numerical study of a single bubble sliding on a downward facing heated surface, J. Heat Transfer 129 (2007) 877–883.
[13] C. Kunkelmann, P. Stephan, Numerical simulation of the transient heat transfer during nucleate boiling of refrigerant HFE-7100, Int. J. Refrig. 33 (2010) 1221–1228.
[14] J.F. Zhao, Z.D. Li, L. Zhang, Numerical simulation on single bubble pool boiling in different gravity conditions, Chin. J. Space Sci. 32 (2012) 537–543.
[15] E. Aktinol, V.K. Dhir, Numerical simulation of nucleate boiling phenomenon coupled with thermal response of the solid, Microgravity Sci. Technol. 24 (2012) 255–265.
[16] L. Zhang, Z.D. Li, K. Li, H.X. Li, J.F. Zhao, Influence of heater thermal capacity on pool boiling heat transfer, J. Comput. Multiph. Flows 6 (3) (2014) 313–327.
[17] Y. Nam, E. Aktinol, V.K. Dhir, Y.S. Ju, Single bubble dynamics on a super-hydrophilic surface with artificial nucleation sites, Int. J. Heat Mass Transfer 54 (7) (2011) 1572–1577.
[18] U. Magrini, E. Nannel, On the influence of the thickness and thermal properties of heating walls on the heat transfer coefficients in nucleate pool boiling, J. Heat Transfer 97 (2) (1975) 173–178.
[19] D.B.R. Kenning, Y. Yan, Pool boiling heat transfer on a thin plate: features revealed by liquid crystal thermography, Int. J. Heat Mass Transfer 39 (15) (1996) 3117–3137.
[20] S. Fischer, S. Herbert, A. Sielaff, E.M. Slomski, P. Stephan, M. Oechsner, Experimental investigation of nucleate boiling on a thermal capacitive heater under variable gravity conditions, Microgravity Sci. Technol. 24 (3) (2012) 139–146.
[21] T. Yabuki, O. Nakabeppu, Study on heat transfer mechanism of isolated bubble nucleate boiling with MEMS sensors, Proceeding of the International Heat Transfer Conference IHTC14, Washington DC, USA, August 8–13, 2010.
[22] Y. Utaka, Y. Kashiwabara, M. Ozaki, Z.H. Chen, Heat transfer characteristics based on microlayer structure in nucleate pool boiling for water and ethanol, Int. J. Heat Mass Transfer 68 (2014) 479–488.
[23] D.Q. Nguyen, R.P. Fedkiw, M. Kang, A boundary condition capturing method for incompressible flame discontinuities, J. Comput. Phys. 172 (1) (2001) 71–98.
[24] W.M. Kays, M.E. Grawford, Convective Heat and Mass Transfer, McGraw-Hill, New York, 1980.
[25] Y.Y. Hsu, On the size range of active nucleation cavities on a heating surface, ASME J. Heat Transfer 84 (1962) 207–216.
[26] J.F. Zhao, Z.D. Li, H.X. Li, J. Li, Thermocapillary migration of deformable drops at moderate to large Marangoni number in microgravity, Microgravity Sci. Technol. 22 (3) (2010) 295–303.
[27] J.F. Zhao, L. Zhang, Z.D. Li, W.T. Qin, Topological structure evolvement of flow and temperature fields in deformable drop Marangoni migration in microgravity, Int. J. Heat Mass Transfer 54 (2011) 4655–4663.
[28] L. Zhang, Z.D. Li, J.F. Zhao, Rebound of liquid droplets caused by sudden decrease of gravity, Interfacial Phenom. Heat Transfer 2 (1) (2014) 41–54.
[29] L. Zhang, Study on the Thermal Dynamical Characteristics of Fluid Particles in Microgravity (Ph.D. thesis), University of the Chinese Academy of Sciences, Beijing, 2014.
[30] R. Siegel, E.G. Keshock, Effects of reduced gravity on nucleate boiling bubble dynamics in saturated water, AIChE J. 10 (4) (1964) 509–516.
[31] W.R. Hu, J.F. Zhao, M. Long, X.W. Zhang, Q.S. Liu, M.Y. Hou, Q. Kang, Y.R. Wang, S.H. Xu, W.J. Kong, H. Zhang, S.F. Wang, Y.Q. Sun, H.Y. Hang, Y.P. Huang, W.M. Cai, Y. Zhao, J.W. Dai, H.Q. Zheng, E.K. Duan, J.F. Wang, Space program SJ-10 of microgravity research, Microgravity Sci. Tech. 26 (3) (2014) 159–169, http://dx.doi.org/10.1007/s12217-014-9390-0.